Journal of Luminescence 248 (2022) 118978

Contents lists available at ScienceDirect

Journal of Luminescence

journal homepage: www.elsevier.com/locate/jlumin

Modulating white light emission temperature in $Ho^{3+}/Yb^{3+}/Tm^{3+}$ triply doped nanostructured GeO_2-Nb_2O_5 materials for WLEDs applications

Vítor dos Santos de Souza, Fábio José Caixeta, Karmel de Oliveira Lima, Rogéria Rocha Gonçalves *

Laboratório de Materiais Luminescentes Micro e Nanoestruturados – Mater Lumen, Departamento de Química, Faculdade de Filosofia, Ciências e Letras de Ribeirão Preto, Universidade de São Paulo, Av. Bandeirantes, 3900, 14040-901, Ribeirão Preto, SP, Brazil

ARTICLE INFO

Keywords:
GeO_2-Nb_2O_5
$GeO_2.9Nb_2O_5$
Rare earth
Sol-gel
Photoluminescence
White emission
Color purity
Correlated color temperature

ABSTRACT

Materials based on $Ho^{3+}/Yb^{3+}/Tm^{3+}$ triply doped with GeO_2-Nb_2O_5 were prepared by the sol-gel methodology followed by thermal annealing at temperatures ranging from 700 to 1100 °C, which affected the crystalline structure and the white light generation of the solids. Trigonal GeO_2 was detected in all the samples, whereas a tetragonal $GeO_2.9Nb_2O_5$ mixed oxide was obtained between 900 and 1100 °C. The spectroscopic properties of the samples depended on the final crystalline structure. When upconversion measurements were performed by using a CW 980 nm laser as excitation source, a cool white light generation was detected for the sample annealed at 900 °C, more specifically; a cool white light has been acquired. In addition, the sample calcined at 1100 °C presented color purity higher than 96% in the yellow-green region where the anti-Stokes process was also being carried out. Excitation with ultraviolet light (245–280 nm) also generated white light. The emitted white light modulation was remarkable. The Cold white light was emitted under shorter wavelengths excitation, whereas warm white light was emitted under longer wavelengths excitation. The outstanding results show the potential of these materials for photonic applications, especially regarding white light emission in solid-state lighting for indoor and outdoor environments.

1. Introduction

White light emission has gained importance in the current society for application in the automotive industry [1], lasers [2–4], cell phone screen displays and flat screen television sets [5–7] and general lighting [8–14]. Due to the evolution and development of new means of illumination, environmentally harmful mercury-based fluorescent lamps have been replaced with diode light emitting devices (LEDs), which present great luminous efficiency, consume less energy, last longer, and are environmentally friendly because they do not contain dangerous elements [15–17].

In 1995, the Nichia Corporation manufactured the first commercial white light LEDs (WLEDs), which combined an InGaN chip emitting in the blue region with a cerium ion-doped YAG matrix ($YAG:Ce^{3+}$) emitting in the yellow region, thereby generating white light [18].

Commercial yellow phosphorus LED does not contain enough red emission component, so this material has high correlated color temperature (CCT >6000 K) and low color rendering index (Ra <80), which limits its use—low CCT and high Ra are essential for indoor lighting applications. One way to overcome this limitation is to develop new materials doped with rare earth ions that emit in the red region. In this context, single-phase matches for white light generation have received increasing researchers' attention [19–21]. Owing to their typical luminescence processes and mechanisms, rare earth matches have become the most useful materials for commercial applications [22]. This makes rare earth ions advantageous for various applications, given their promising vast properties in photocatalysis [23], optical thermometer [24], and especially in solid-state lighting [25], which is one of the focuses of this work.

WLEDs emit white light through three different processes: (1) LED chips excited in the ultraviolet region emit in the blue, green, and red regions; (2) blue LED chips are used to obtain yellow emission or a combination of green and red emissions, associated with the blue emission generated by the LED chip; and (3) red, green, and blue (RGB) emissions can be combined [15,18].

On the basis of the RGB system, white light can also be generated by

* Corresponding author.
E-mail address: rrgoncalves@ffclrp.usp.br (R.R. Gonçalves).

https://doi.org/10.1016/j.jlumin.2022.118978
Received 19 October 2021; Received in revised form 2 May 2022; Accepted 5 May 2022
Available online 7 May 2022

excitation in the ultraviolet region, or in the near infrared excitation followed by an upconversion via incorporation of rare earth ions into inorganic hosts in both the thin film and oxides powder forms. Concerning solid-state light, oxides have been widely explored as matrixes for luminescent materials because they have wide bandgap, are easy to synthesize and to handle, and present high structural and thermal stability [26]. In view of this information, synthesizing a material based on GeO_2-Nb_2O_5 doped with Ho^{3+}, Yb^{3+}, and Tm^{3+} to investigate its spectroscopic properties for white light emission would be interesting.

GeO_2 is highly transparent in the infrared region, with refractive index (n) of 1.7–1.8 and bandgap of 3.5–4.0 eV. Glassy and glass-ceramic germanium-based materials have interesting properties for use as arrays of optical amplifiers. Moreover, the phonon energy of these materials (~880 cm^{-1}) is lower than other glassy materials such as silicate (~1100 cm^{-1}), phosphates (~1200 cm^{-1}), and borates (~1400 cm^{-1}). Low phonon energy is a desirable feature, once it reduces the probability of non-radioactive processes when they are doped with rare earth ions [27]. In addition, glassy and glass-ceramic germanium-based materials have additional properties that favor their application, for instance, as micropattern photogravings for use in photonic devices [28].

Nb_2O_5 has low phonon energy (~700 cm^{-1}) [29], high dielectric constant, broad bandgap of 3.6 eV, and high refractive index (n = 2.4) [30]. Nb_2O_5 has been employed in various vitreous systems doped with rare earth ions. Indeed, addition of rare earth ions to this oxide improves the oxide structure by increasing its refractive index and decreasing the phonon energy and by promoting solubilization of the rare earth ions and reducing the OH groups, directly affecting the optical and luminescent properties of the oxide [31,32].

In this work, we have been demonstrating the viability of stabilizing an interesting rare earth host based on mixed oxide structure of GeO_2 and Nb_2O_5, in which the white light emission temperature can be modulated.

2. Experimental procedure

2.1. Synthesis of materials

The Ho^{3+}/Yb^{3+}/Tm^{3+} triply doped GeO_2–Nb_2O_5 materials were prepared by the well-known sol–gel methodology. A solution of 20.0 mL of Ge/Nb at 70:30 M ratio and total Ge + Nb concentration of 0.448 mol L^{-1} was employed. The molar concentration (mol%) of the dopants was calculated by considering the number of moles of Ge + Nb equal to 100%, to provide mol% concentrations of 0.3, 1.2, and 0.5 of Ho^{3+}, Yb^{3+}, and Tm^{3+}, respectively. The Nb^{5+} ethanolic solution was obtained as described in detail by CAIXETA et al. [33]. To this end, optical grade Nb_2O_5 (99.9%) supplied by Companhia Brasileira de Metalurgia e Mineração (CBMM) was dissolved in concentrated hydrochloric acid (HCl, Panreac, 37 wt%) under stirring at 70 °C for 5 h, followed by drying at 80 °C and addition of anhydrous ethanol (Merck – 99.9%). A final 0.2 mol L^{-1} Nb^{5+} ethanolic solution was obtained. The ethanolic chloride solutions of the dopants were prepared by dissolving the respective oxides (Ho_2O_3, Yb_2O_3, and Tm_2O_3; Sigma–Aldrich, 99.9%) in concentrated HCl (Panreac, 37 wt%) (Yb^{3+} and Tm^{3+}) or concentrated nitric acid (HNO_3, Sigma–Aldrich, 65 wt%) (Ho^{3+}) under stirring at 70 °C for 3 h, followed by drying at 80 °C and addition of anhydrous ethanol (Merck – 99.9%). The Ln^{3+} obtained solutions were titrated by ethylenediaminetetraacetic acid (EDTA) complexation and using xylenol orange as an indicator.

The final solution was prepared by using two containers. In the first container, GeO_2 (99.999%, Sigma–Aldrich) was solubilized in 25 wt% tetramethylammonium hydroxide solution (TMAH; Sigma–Aldrich, 25 wt%) in water under agitation, with subsequent addition of acetylacetone. In the second container, Nb^{5+} chloride ethanolic solutions and doping solutions of Yb^{3+} and Tm^{3+} chloride and Ho^{3+} nitrate (in the proportions mentioned above) were added. Then, the contents of the second container were added to the first container under stirring at room temperature. Subsequently, concentrated HNO_3 (Sigma–Aldrich, 65 wt %) was added until pH 4.0 was reached. A white precipitate was obtained, dried in an oven at 60 °C for 24 h, and thermally titrated at 700, 900, and 1100 °C for 3 h.

The isolated $GeO_2.9Nb_2O_5$ triply doped with 0.3% Ho^{3+}, 1.2% Yb^{3+} and, 0.5% Tm^{3+} was synthesized under the same conditions previously described. Molar ratio of 5.3:94.7 for Ge:Nb has been employed. The obtained solid was annealed at 900 °C for 3 h.

2.2. Characterizations

The powder X-ray diffractograms were obtained on a Siemens–-Bruker D5005–AXS diffractometer operating with CuKα radiation of 1.5406 Å, graphite monochromator, step of 0.02° s^{-1}, and 2θ ranging from 5 to 90°. The Transmission electron microscopy (TEM) images were acquired at 100 kV in a JEOL JEM-100CX II microscope. The samples were prepared by drop-casting powder dispersion in pure ethanol on TEM copper grids covered with carbon.

The vibrational spectra in the infrared region with Fourier Transform (FTIR) were acquired from 400 to 4000 cm^{-1} on a Shimadzu IR Prestige–21 spectrometer, with a resolution of 2 cm^{-1}; KBr pellets were used.

Photoluminescence analyses in the visible region were performed at ambient temperature on a Horiba Scientific Fluorolog 3 spectrofluorometer (model FL3–22) equipped with a double monochromator H10330–75, uncooled, with detection at 22.5°. For the excitation spectra from 240 to 280 nm and resolved in time, a continuous and pulsed Xe lamp of 450 W was used, respectively. To obtain the upconversion spectra of the samples, a CW diode laser of 980 nm (DMC Group) was employed; the following power values were used: 218, 262, 302, 343, 383, 424, 511, 595, 706, and 812 mW.

3. Results and discussion

3.1. Structural properties

Fig. 1 shows the diffractograms of the GeO_2–Nb_2O_5:Ho^{3+}/Yb^{3+}/Tm^{3+} nanocomposite annealed at 700, 900, and 1100 °C for 3 h. At 700 °C, crystallization was evident as indicated by the peaks at 20°, 26°, 38°, 41°, 48°, and 59°, which are assigned to the crystalline structure of trigonal GeO_2. Such structure has lattice parameters a = 4.995 Å, b = 4.995 Å, c = 5.649 Å, angles α = β = 90° and γ = 120°, and spatial group $P3_121$ (JCPDS 01–073–9110), corresponding to α-GeO_2 [34,35].

When the GeO_2-Nb_2O_5:Ho^{3+}/Yb^{3+}/Tm^{3+} nanocomposite was annealed at 900 or 1100 °C for 3 h, additional peaks appeared at 23°, 25°, 34°, 44°, and 58°. These peaks have been reported for a niobium and germanium mixed oxide, $GeO_2.9Nb_2O_5$ [36], with tetragonal structure, lattice parameters a = 15.736 Å, b = 15.736 Å, and c = 3.827 Å, angles α = β = γ = 90°, and space group I 4/m (JCPDS 01–070–1697).

It is worth noting that the mixed oxide $GeO_2.9Nb_2O_5$, obtained by the possible stabilization in temperatures from 900 °C shows the possibility of exploring this phase as a host of rare earths. CAIXETA et al. [28] have been working on GeO_2-Ta_2O_5 doped systems analogous to GeO_2-Nb_2O_5, which shows singular results as a rare earth host with applications in real-time temperature sensor and photothermal conversion.

Fig. 2 displays TEM images of the GeO_2-Nb_2O_5:Ho^{3+}/Yb^{3+}/Tm^{3+} nanocomposite annealed at 900 or 1100 °C. After annealing at 900 °C (Fig. 2A) it has been observed the formation of a nanostructured material by the dispersion of Nb_2O_5 nanocrystals into GeO_2-based host. AQUINO et al. [37] observed a similar material formation for SiO_2–Nb_2O_5, where Nb_2O_5 nanocrystals are embedded in the SiO_2 amorphous structure. On the other hand, TEM images of GeO_2-Nb_2O_5: Ho^{3+}/Yb^{3+}/Tm^{3+} annealed at 1100 °C (Fig. 2B) depict the massive presence of GeO_2 crystals on the nanocomposite surface, what is in agreement to XRD results, i.e., higher crystallization fraction at 1100 °C

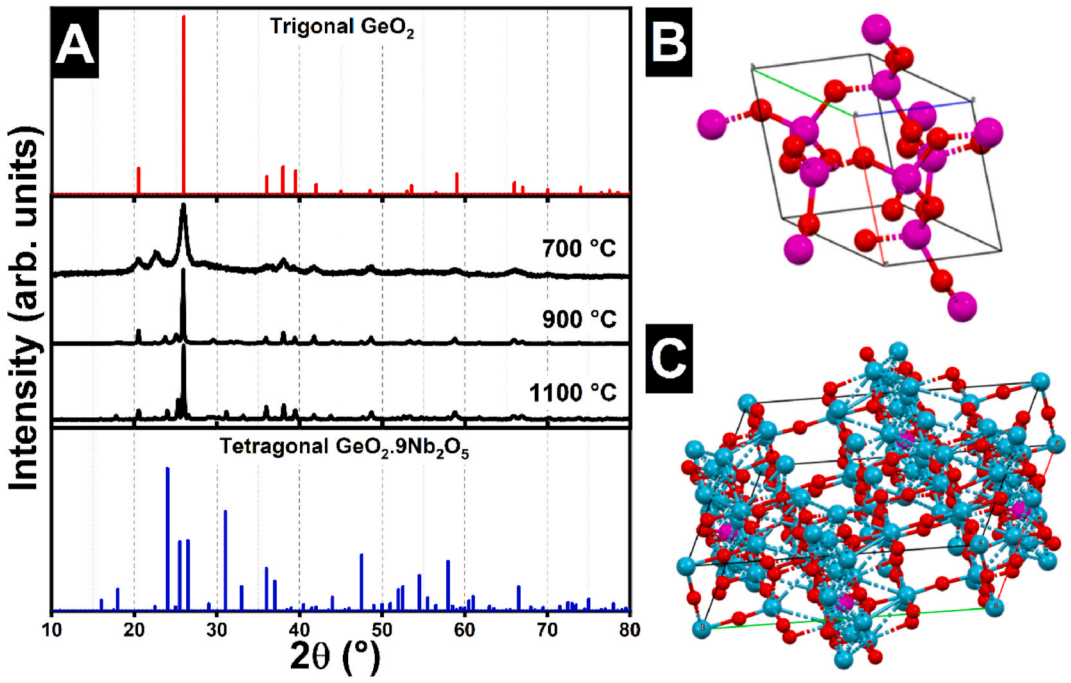

Fig. 1. Diffractograms of the $Ho^{3+}/Yb^{3+}/Tm^{3+}$ triply doped GeO_2-Nb_2O_5 nanocomposite annealed at 700, 900, and 1100 °C for 3 h and patterns of the trigonal GeO_2 in red and the tetragonal $GeO_2.9Nb_2O_5$ in blue (A). Unit cells of trigonal GeO_2 (B) and tetragonal $GeO_2.9Nb_2O_5$ (C) obtained by using Mercury® (Mercury CSD version 4.3.1, 2020).

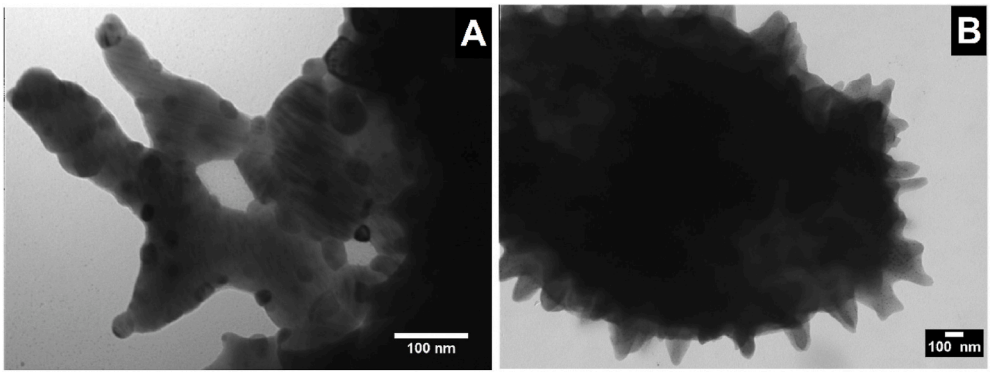

Fig. 2. TEM Images of nanocomposite GeO_2-Nb_2O_5:$Ho^{3+}/Yb^{3+}/Tm^{3+}$ calcined at (A) 900 or (B) 1100 °C.

than 900 °C.

The presence of GeO_2 crystals on the nanocomposite surface, as shown in Fig. 2B, is favored by the high proportion of germanium used in the synthesis. As the electronic density of GeO_2 is lower than the Nb_2O_5 one, the GeO_2 crystals appear white light color contrast in the TEM image. The same was verified by Balitsky et al. [38], where the growth of germanium oxide crystals with the same morphology as the one obtained in the present work has been observed.

FTIR analysis (Fig. 3) of GeO_2-Nb_2O_5:$Ho^{3+}/Yb^{3+}/Tm^{3+}$ without thermal treatment (WTT) and calcined at 700, 900, and 1100 °C for 3 h was carried out. Table 1 shows the assignments. Disappearance of the bands due to the vibrational modes of CH_3–N^+ (trimethylammonium ion) indicated that increasing thermal treatment temperature removed organic matter. The vibrational modes of the OH groups also disappeared, indicating water loss. Bands corresponding to impurities, such as OH in the 4000–3000 cm^{-1} region, must be eliminated because these impurities suppress or reduce luminescence [31]. Increasing treatment temperature intensified the bands due to the GeO_2 and Nb_2O_5 vibrational modes, indicating that these oxides were formed and confirming the X-ray diffraction results.

3.2. Photoluminescent properties

Fig. 4 shows the upconversion (UC) spectra of the samples calcined at 700, 900, and 1100 °C under excitation with a 980-nm continuous laser; the following powers were used: 812, 706, 595, 511, 424, 383, 343, 302, 262, and 218 mW. The spectra were recorded from 380 to 900 nm.

The spectral profile of the sample thermally treated at 900 °C (Fig. 3B) resembled the spectral profile of Y_2O_3:$Ho^{3+}/Yb^{3+}/Tm^{3+}$ depicted by PANDEY & RAI [46], the emission in the blue region at 470 nm is related to and $^1G_4 \rightarrow {}^3H_8$ transition of Tm^{3+} ions. Contribution to the emission in the green region was evidenced by the $^2S_2, {}^6F_4 \rightarrow {}^6I_8$ (544

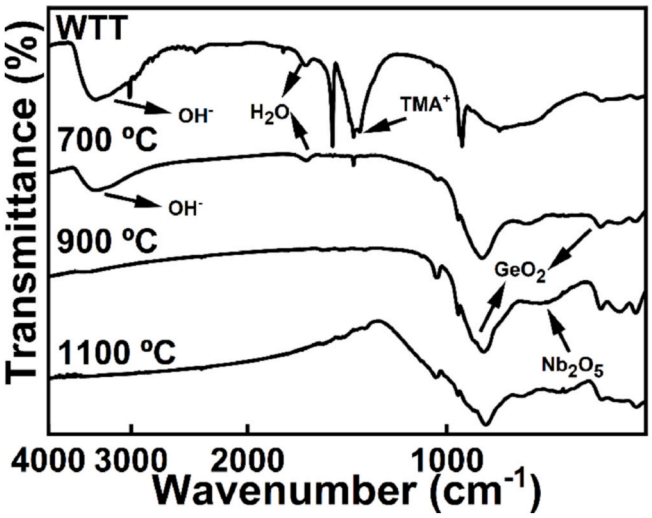

Fig. 3. FTIR band assignment for the $Ho^{3+}/Yb^{3+}/Tm^{3+}$ triply doped GeO_2-Nb_2O_5 nanocomposite without thermal treatment (WTT) and annealed at 700, 900, and 1100 °C for 3 h.

Table 1
FTIR bands and their assignments.

Wavenumber (cm^{-1})	Assignment	Reference
3700–2560	OH^-	[39]
1628	H_2O	[39]
1488, 1472-1247	CH_3–N^+	[40,41]
1089–789	GeO_2	[42,43]
780-633, 613-500	Nb_2O_5	[39,44,45]

nm) transition of Ho^{3+} ions, and the emission in the red region can be attributed to the $^5F_6 \rightarrow {}^6I_8$ (660 nm) transition of Ho^{3+} ions and $^1G_4 \rightarrow {}^3F_4$ transition (645 nm) of Tm^{3+} ions. Emission was also observed in the near infrared (NIR) due to the $^3H_4 \rightarrow {}^3H_6$ transition (800 nm) of Tm^{3+} ions.

In contrast to the spectrum of the sample thermally treated at 900 °C, the spectrum of the sample thermally treated at 1100 °C (Fig. 4C) displayed emissions in the green (544 nm), red (645 and 660 nm), and near infrared (800 nm) regions, but not in the blue region. For the sample thermally treated at 700 °C, Fig. 4A revealed the same emissions in the green and red regions. In this case, the low intensity of the emissions could be due to the fact that OH groups were still present at this treatment temperature (as shown in Fig. 3), suppressing the luminescence. Because Yb^{3+} ions have a high cross-section, they can act as sensitizers, absorbing photons and transferring their energy to the Tm^{3+} or Ho^{3+} ions. As a result, blue, green, and red emissions are achieved, further contributing to white light emission [47].

There is a possible influence of formation of the mixed oxide on the spectroscopic properties, featuring a dependency upconversion emission with structure. In the spectra, of Fig. 4C and 4 B, the heat-treated samples above 900 °C show the appearance of mixed oxide, the emission in the visible region is more favored when compared to the emission in the infrared (~800 nm). It is worth drawing attention to the material exhibits evidence of an upconversion high yield similar to the analog system GeO_2-Ta_2O_5 [28].

As previously shown and discussed, the increase in the treatment temperature favors the crystallization process; and more specifically at 1100 °C the formation of tetragonal $GeO_2.9Nb_2O_5$ is clearly observed. Because of such crystallization increase, shorter distances between the rare earth ions occur and energy transfer between them is favored. In this sense, cross relaxation process can lead to emissions in green and red regions, and it disables emission processes in the blue.

CIE 1931 chromaticity diagrams were constructed for all the

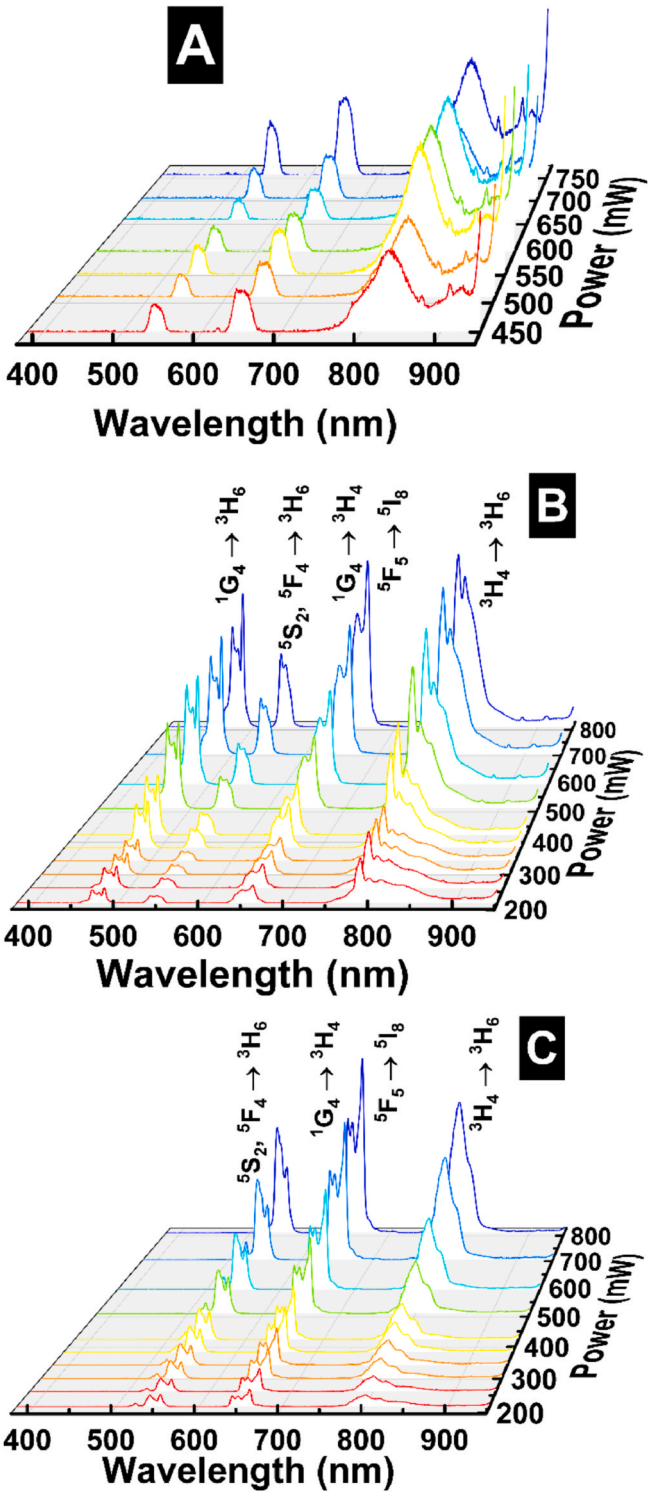

Fig. 4. Upconversion emission spectra of the $Ho^{3+}/Yb^{3+}/Tm^{3+}$ triply doped GeO_2-Nb_2O_5 nanocomposite annealed at (A) 700, (B) 900, and (C) 1100 °C for 3 h, under 980-nm excitation.

samples, irrespective of the treatment temperature. The diagram obtained for the sample thermally treated at 900 °C (Fig. 5B) indicated emission in the white light region and had contributions from blue, green, and red emissions responsible for white light in RGB systems. The samples thermally treated at 700 or 1100 °C (Fig. 4A and C, respectively) only had emissions in the green and red regions, without blue contribution for emission in the yellow-green region.

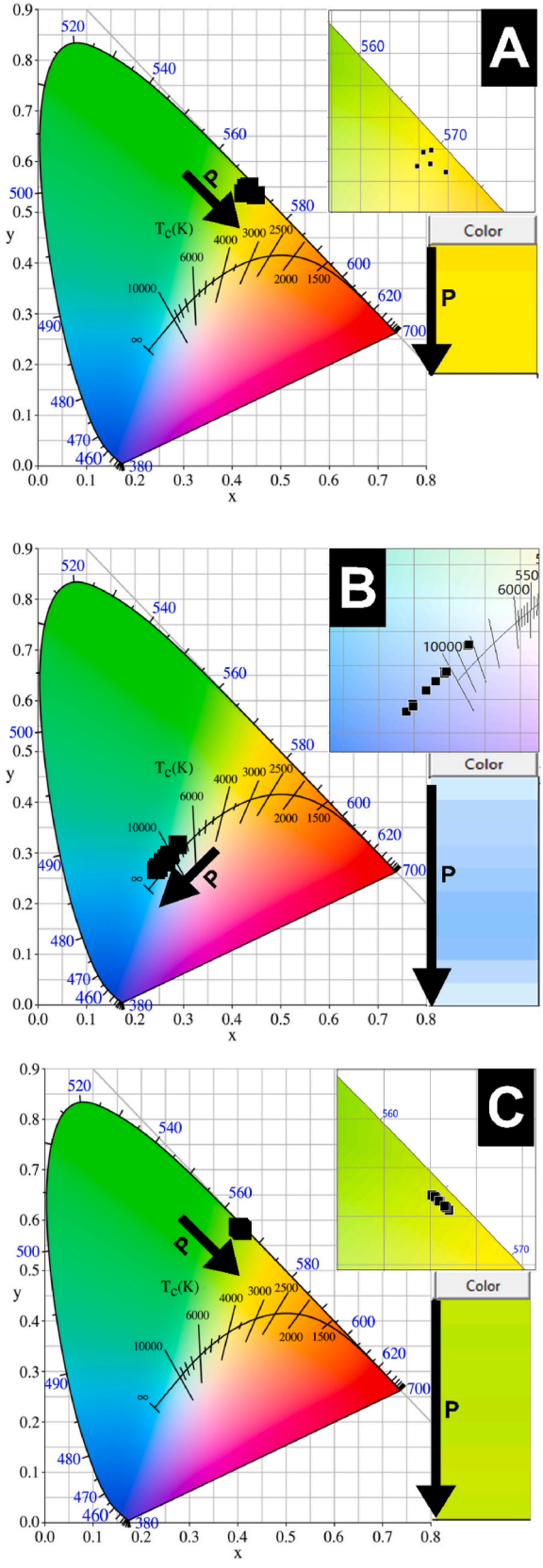

Fig. 5. CIE 1931 chromaticity diagrams of the $Ho^{3+}/Yb^{3+}/Tm^{3+}$ triply doped GeO_2-Nb_2O_5 nanocomposite annealed at (A) 700, (B) 900, and (C) 1100 °C for 3 h. The arrow (→) indicates the increase in the excitation power (P). The chromaticity diagrams were obtained from the upconversion emission spectra presented in Fig. 4; the OSRAM ColorCalculator® program (version 7.23, 2020) was employed.

The emission of the samples was also evaluated by calculating the color purity (CP), obtained with the coordinate points located close to the edges of the chromaticity diagram, where CP is 100%, the so-called *Laser Locus*, and equation (1) [48–50], where (x, y) are the color coordinates of the sample, (x_i, y_i) are the chromaticity coordinates of the white emission (0.333, 0.333), and (x_d, y_d) are the coordinates of the dominant wavelength in 565 nm with coordinates (0.4087, 0.5896), as seen in Fig. 4C.

$$color\ purity = \sqrt{\frac{(x-x_i)^2+(y-y_i)^2}{(x_d-x_i)^2+(y_d-y_i)^2}} * 100\% \quad (1)$$

Table 2 exhibits the coordinates of the CIE 1931 chromaticity diagram and color purity for a sample doped with $Ho^{3+}/Yb^{3+}/Tm^{3+}$ and thermally treated at 1100 °C, under excitation at 980 nm. The sample showed yellow-green emission with color purity close to 96% at all excitation powers and under excitation at 980 nm, which indicated that the material has several potential photonic applications.

Fig. 6 depicts the transitions of the $Ho^{3+}/Yb^{3+}/Tm^{3+}$ ions and the energy transfers between the Yb^{3+}→Ho^{3+} and Yb^{3+}→Tm^{3+} ions under excitation at 980 nm.

Under excitation at 980 nm, the Yb^{3+} ions can absorb a photon and be excited to the $^2F_{5/2}$ state. Next, these ions transfer their energy to the Tm^{3+} ions, which are excited to the $^3H_5$ state. The Tm^{3+} ions in the $^3H_5$ state can lose energy non-radioactively and reach the $^3F_4$ state, where they may receive another photon through energy transfer from the Yb^{3+} ions and reach the $^3F_{3,2}$ state. In the latter state, the Tm^{3+} ions can lose energy non-radioactively and reach the $^3H_4$ state, from where they reach the ground state ($^3H_6$) by emitting light at 800 nm. Also, the Yb^{3+} ions can transmit another photon to the Tm^{3+} ions, raising their energy to the $^1G_4$ state. After that, emission in the red region at 645 nm in a two-photon system takes the Tm^{3+} ions to the $^3F_4$ state, or emission in the blue region at 470 nm in a three-photon system takes the Tm^{3+} ions to the $^3H_6$ state [51].

A similar situation occurs with the Ho^{3+} ions. Energy transfer from the Yb^{3+} ions excites the Ho^{3+} ions to the $^5I_6$ state. In this state, the Ho^{3+} ions can receive another photon and have their energy raised to the $^5S_2$,$^5F_4$ states. Emission in the green region at 544 nm takes the Ho^{3+} ions to the ground state ($^5I_8$) in a two-photon system. In addition, the Ho^{3+} ions in the $^5I_6$ state can lose energy non-radioactively until they reach the $^5I_7$ state, where they can gain energy from the Yb^{3+} ions and be excited to the $^5F_5$ state, to emit in the red region at 660 nm in a two-photon system and reach the ground state [52,53].

From the UC spectra, the number of photons involved in the emissions in the blue, green, and red regions was determined by the power law $I \alpha P^n$, where I is the intensity of the emissions, P is the applied power, and n is the number of photons involved in the upconversion process [51]. In this way, a graph of log power versus log emission area was constructed for GeO_2–Nb_2O_5:$Ho^{3+}/Yb^{3+}/Tm^{3+}$, to determine the number of photons (Fig. 6).

Table 2
CIE 1931 chromaticity coordinates and color purity of the $Ho^{3+}/Yb^{3+}/Tm^{3+}$ triply doped GeO_2-Nb_2O_5 nanocomposite annealed at 1100 °C, under excitation at 980 nm at different laser powers.

Power (mW)	Color coordinates		Color Purity (%)
	x	y	
262	0.406	0.583	97.2
302	0.401	0.586	97.9
343	0.405	0.583	97.1
383	0.403	0.585	97.7
424	0.403	0.585	97.7
511	0.405	0.583	97.1
595	0.410	0.578	96.1
706	0.409	0.579	96.1
812	0.408	0.580	96.5

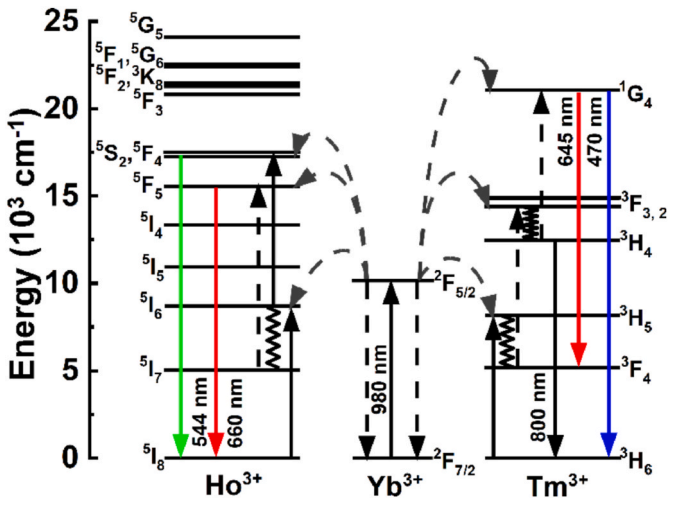

Fig. 6. Energy levels diagram of Ho^{3+}, Yb^{3+}, and Tm^{3+} ions and excitation/emission mechanisms for emissions in the visible region after 980-nm irradiation.

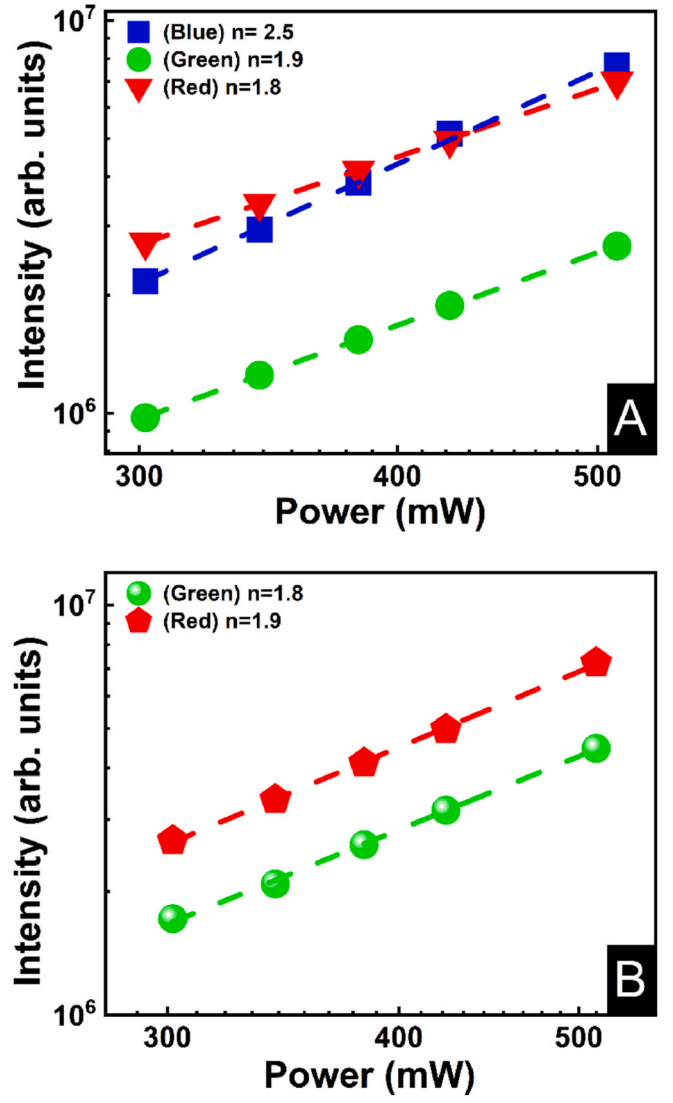

Fig. 7. Log-log plots of integrated emission area vs. power for the $Ho^{3+}/Yb^{3+}/Tm^{3+}$ triply doped GeO_2-Nb_2O_5 nanocomposite annealed for at (A) 900 °C and (B) 1100 °C for 3 h.

Fig. 7A displays the number of photons obtained for the sample treated at 900 °C, for the blue region (n = 2.5), for the green region (n = 1.9), and for the red region (n = 1.8). As for the number of photons for the sample thermally treated at 1100 °C, Fig. 7B revealed n = 1.8 for the green region and n = 1.9 for the red region. The number of photons close to 3 for emissions in the blue region and close to 2 for emissions in the green and red regions indicated the mechanism of energy transfer from the Yb^{3+} to the Ho^{3+} ions accounting for emissions in the green, and red regions and from the Yb^{3+} to the Tm^{3+} ions accounting for emissions in the blue and red regions. The variations in the slopes of the number of photons that caused a decimal deviation in their values were attributed to the competition between the linear decay and the upconversion process for depletion of the excited intermediate states and to the local thermal effect [54].

Fig. 8 displays the emission spectra of the GeO_2-Nb_2O_5:$Ho^{3+}/Yb^{3+}/$

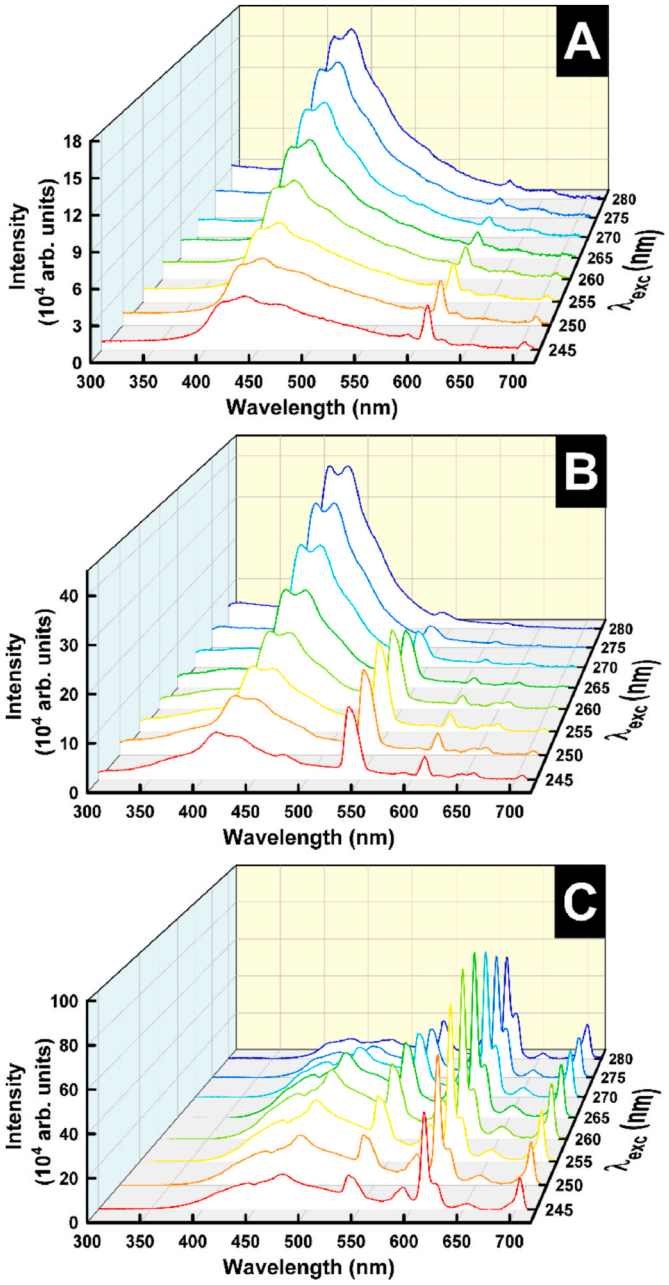

Fig. 8. Emission spectra of $Ho^{3+}/Yb^{3+}/Tm^{3+}$ triply doped GeO_2-Nb_2O_5 nanocomposite annealed at (A) 700, (B) 900, and (C) 1100 °C for 3 h, under UV excitation.

Tm^{3+} nanocomposite annealed at 700, 900, and 1100 °C under UV excitation. The spectra were collected between 300 and 720 nm after excitation from 245 to 280 nm. All the spectra presented a broad band from 360 nm to approximately 600 nm, which overlapped some rare earth ion transitions depending on the thermal treatment. This broad band was attributed to emission of the GeO_2-Nb_2O_5 host lattice. For the annealing temperature of 1100 °C (Fig. 8C), the emission band of the host lattice reduced significantly. Moreover, the spectral profile changed due to formation of $GeO_2.9Nb_2O_5$ at this temperature, as previously discussed in the XRD results.

In addition to the emission band of the host lattice, the emissions of the Ho^{3+} ions at 540, 590, 613, 623, and 653 nm were observed, attributed to the $^5S_2$, $^5F_4 \rightarrow {}^5I_8$, $^5G_6 \rightarrow {}^5I_7$, $^5F_2 \rightarrow {}^5I_7$, $^5F_3 \rightarrow {}^5I_7$, and $^5F_5 \rightarrow {}^5I_8$ transitions, respectively [55,56]. The emissions of the Tm^{3+} ions referring to the $^1G_4 \rightarrow {}^3F_4$ (653 nm) and $^3F_3 \rightarrow {}^3H_6$ (704 nm) transitions [57] favored the transitions of both ions with increasing treatment temperature, precisely because OH groups and organic matter, which suppress luminescence, were eliminated. Fig. 9 shows the diagram representing the energy levels under excitation in the ultraviolet (245–280 nm) region.

It is also observed that in the emission spectra with excitation in the UV the emission in the visible region due to the rare earth ions is favored when the treatment temperature increases, this is due to the formation of the mixed oxide. At 1100 °C, the temperature at which a greater formation of mixed oxide occurs, a very large influence of its presence on the white emission is noted, which shows the chromaticity diagrams in Fig. 10.

With excitation in the UV, the host lattice is excited and both its emission and that of rare earth ions occur. With the increase in the treatment temperature, which results in an increase in the formation of mixed oxide, the transfer of energy between the host network and the rare earth ions is favored given the intensity of the transitions. Consequently, there is a reduction of non-radioactive processes that also favor the emission of ions, since there will be no more loss by non-radioactive processes. In this way, the formation of the mixed oxide phase favors the quantum yield as well as in the analogous system of GeO_2-Ta_2O_5 [28], besides also favoring the white emission, which corroborates with the previous data of Upconversion.

CIE 1931 chromaticity diagrams were constructed for the samples treated at the three different annealing temperatures. The samples thermally treated at 700 or 900 °C (Fig. 10A and B, respectively) emitted in the blue region because they presented great contribution from the

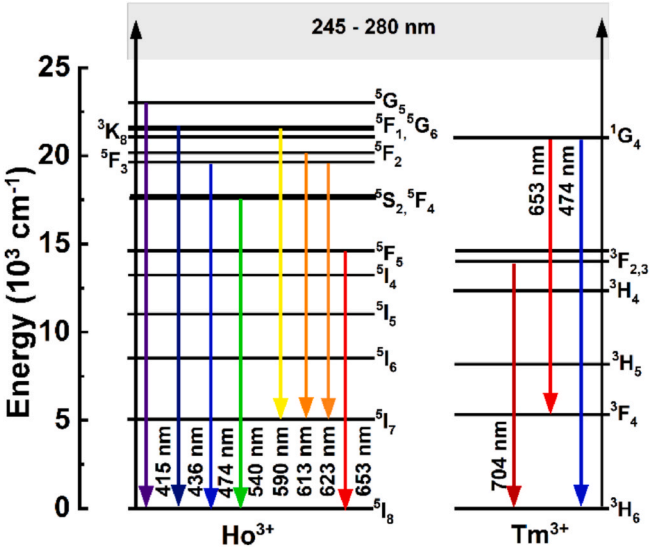

Fig. 9. Energy levels diagram of the Ho^{3+} and Tm^{3+} ions and excitation/emission mechanisms in the UV (245–280 nm) and visible regions.

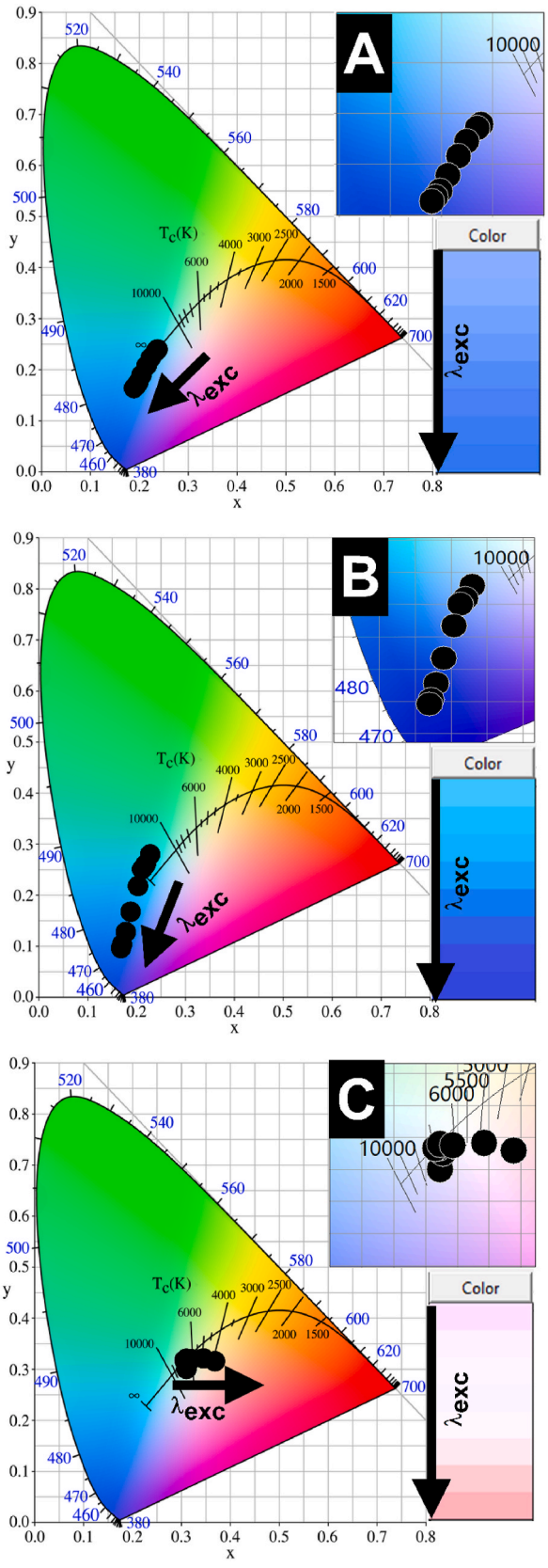

Fig. 10. CIE 1931 chromaticity diagrams of the $Ho^{3+}/Yb^{3+}/Tm^{3+}$ triply doped GeO_2-Nb_2O_5 nanocomposite annealed at (A) 700, (B) 900, and (C) 1100 °C for 3 h. The arrow (→) indicates the increase in the excitation wavelength (λ_{exc}). The chromaticity diagrams were obtained from the upconversion emission spectra presented in Fig. 8; the SRAM ColorCalculator® program (version 7.23, 2020) was used.

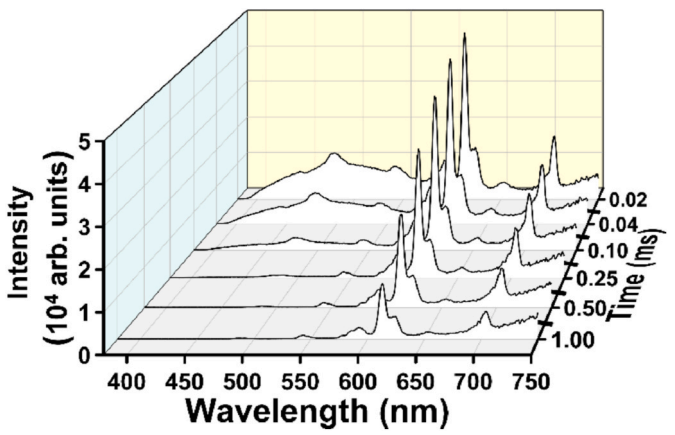

Fig. 11. Time-resolved emission spectra of the $Ho^{3+}/Yb^{3+}/Tm^{3+}$ triply doped GeO_2-Nb_2O_5 nanocomposite annealed at 1100 °C for 3 h, after excitation at 260 nm.

host lattice broadband emission compared to the emission of the rare earth ions. Fig. 10C illustrates the chromaticity diagram of the sample calcined at 1100 °C, which emitted in the region of light generation under excitation with light in the region of 245–280 nm.

To obtain more information about the white emission of the GeO_2-Nb_2O_5:$Ho^{3+}/Yb^{3+}/Tm^{3+}$ nanocomposite, time-resolved emission measurements were carried out for the sample annealed at 1100 °C. Fig. 11 depicts the spectra obtained after excitation at 260 nm and delay time of 0.02, 0.04, 0.1, 0.25, 0.5, and 1 ms. Increasing delay time decreased the intensity of the broadband located in the region of 380–550 nm. Such result proved that this band referred to emission of the host lattice, given that this emission has shorter lifetime than the emission of rare earth ions [58]. The emission at 480 nm was related to both the Tm^{3+} $^1G_4 \rightarrow {}^3H_6$ [57] and Ho^{3+}:$^5F_3 \rightarrow {}^5I_8$ [59] transitions and pronounced, confirming the presence of such transitions upon reduction of the emission band of the host lattice.

The Correlated color temperature (CCT) expressed in absolute temperature (K) is defined as the temperature of a blackbody emitter in which the CIE coordinate (x, y) is close to the CIR coordinate (x, y) of the light in comparison. A blackbody emitter with emissions in the orange-red, yellow, white, and bluish-white regions has the same characteristic profile as a visible light source; that is, the CCT is important to characterize the spectral properties of systems that emit white light in the specific case of application in lighting LED systems. CCT values ranging from 2700 to 5000 K correspond to warm colors, from red to yellowish white, and are widely used and suitable for lighting intimate spaces like dining rooms, living rooms, rooms, and restaurants. CCT values above 5000 K correspond to bluish white, or cool, colors, which are ideal for lighting environments such as hospitals, offices, and kitchens [60,61].

Table 3
CIE 1931 chromaticity coordinates and CCT values of the $Ho^{3+}/Yb^{3+}/Tm^{3+}$ triply doped GeO_2-Nb_2O_5 nanocomposite annealed at 900 °C, under excitation at 980 nm.

Power (mW)	Color coordinates		CCT (K)
	x	y	
218	0.288	0.315	8,299
262	0.272	0.295	10,596
302	0.272	0.294	10,664
343	0.266	0.288	11,912
383	0.258	0.281	13,795
424	0.249	0.271	17,935
511	0.244	0.266	21,606
595	0.250	0.270	18,303
706	0.273	0.295	10,416
812	0.290	0.315	8,202

To calculate CCT values, equation (2), known as McCamy's formula, and the CIE Coordinates of the emitting material are used [62]:

$$CCT = 449n^3 + 3525n^2 + 6823.3n + 5520.3 \quad (2)$$

where, $n = \frac{x-0.3320}{0.1858-y}$

Next, the coordinates (x, y) of the CIE 1931 chromaticity diagrams of the samples that presented emission in the white light region; that is, the sample thermally treated at 900 °C under excitation at 980 nm (Table 3) and the sample thermally treated at 1100 °C under excitation in the ultraviolet region (245–280 nm) were obtained (Table 4).

Under excitation at 980 nm, the sample thermally treated at 900 °C had CCT value higher than 5000 K, which indicated that emission was cold white. Under excitation in the ultraviolet region up to 270 nm, the sample thermally treated at 1100 °C also had cold white emission. However, when the material was excited at 275 and 280 nm, the CCT values were lower than 5000 K, emission was warm white. This change occurred because the intensity of the blue regions decreased when compared to the other excitation lengths [61]. In other words, warm white or cold white emission can be controlled by changing the excitation wavelength.

3.3. Structural, morphological and spectroscopic properties of $GeO_2.9Nb_2O_5$

In order to obtain more information about the influence of the mixed oxide ($GeO_2.9Nb_2O_5$) on the spectroscopic properties of $Ho^{3+}/Yb^{3+}/Tm^{3+}$ triply doped GeO_2-Nb_2O_5 system. The synthesis of the $Ho^{3+}/Yb^{3+}/Tm^{3+}$ triply doped $GeO_2.9Nb_2O_5$ nanocomposite was performed in order to isolate only this crystalline phase. Fig. 12 presents the diffractograms and TEM images of the tetragonal nanocomposite $GeO_2.9Nb_2O_5$:$Ho^{3+}/Yb^{3+}/Tm^{3+}$, the peaks clearly show the formation of pure mixed oxide formation (JCPDS 01–070–1697) annealed at 900 °C for 3 h. The crystallite size (τ) was calculated using equation (3) [63].

$$\tau = \frac{0.9\lambda}{(\beta_s - \beta_i)cos\theta} \quad (3)$$

where, 0.9 is the Scherrer constant for the spherical shape of the crystallite, λ = 1.5406 Å (K_α radiation of Cu), β_s = integrate area/intensity from the peak of the sample, β_i = integrate area/intensity of the correction for the instrumental broading.

The calculation was performed using the area of the peaks at 18°, 25°, 30°, 32° and 36° (indicated by (*) in the diffractogram in Fig. 12) by deconvolution using the Pseudo-Voigt function [64], obtaining mean size value of crystallite equal to 14.89 nm. The crystallite size comparison of $GeO_2.9Nb_2O_5$: $Ho^{3+}/Yb^{3+}/Tm^{3+}$ with other oxides systems is shown in Table 5.

The crystallite size value obtained for the $GeO_2.9Nb_2O_5$:$Ho^{3+}/Yb^{3+}/Tm^{3+}$ nanocomposite is similar to the values obtained in the literature ranging from 8.8 to 15 nm (Table 5) for different systems with two and/or three oxides in its structure. The TEM image also presented in Fig. 12,

Table 4
CIE 1931 chromaticity coordinates and CCT values of the $Ho^{3+}/Yb^{3+}/Tm^{3+}$ triply doped GeO_2-Nb_2O_5 nanocomposite annealed at 1100 °C, under excitation from 245 to 280 nm.

Excitation (nm)	Color coordinates		CCT (K)
	x	y	
245	0.311	0.300	6,893
250	0.314	0.313	6,591
255	0.311	0.317	6,721
260	0.308	0.317	6,916
265	0.312	0.320	6,650
270	0.321	0.319	6,087
275	0.346	0.320	4,806
280	0.370	0.315	3,768

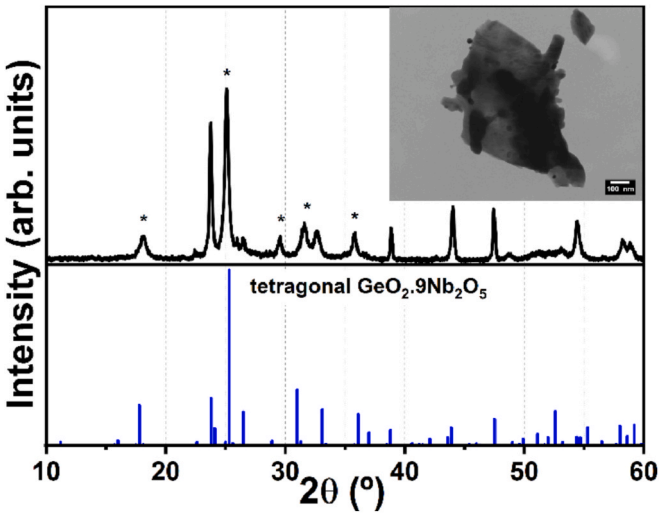

Fig. 12. Diffractograms and TEM image of tetragonal $GeO_2.9Nb_2O_5$:Ho^{3+}/Yb^{3+}/Tm^{3+} nanocomposite annealed at 900 °C for 3 h (*) Crystal planes used to calculate crystallite size.

Table 5
Crystallite size of some oxides systems found in the literature.

Sample	Scherrer's crystallite size (nm)	Reference
$GeO_2.9Nb_2O_5$:Ho^{3+}/Yb^{3+}/Tm^{3+}	14.89	This work
$70SiO_2$–$30Nb_2O_5$:0.3 Tm^{3+}, 1.2 Yb^{3+}	10.00	[65]
$60SiO_2$–$40Nb_2O_5$:0.3Er^{3+}, 1.2 Yb^{3+}	12.70	[44]
$50SiO_2$–$50Ta_2O_5$:0.3Er^{3+}	11.40	[66]
$70SiO_2$-$30HfO_2$:1Er^{3+}	8.80	[67]
$75GeO_2$-$15Nb_2O_5$–$10K_2O$	15.00	[68]
$35SiO_2$–$15Al_2O_3$-$50GeO_2$:1Er^{3+}	12.00	[69]

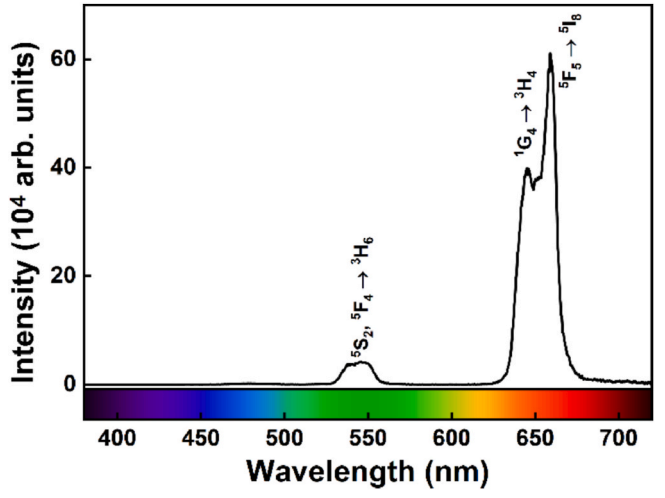

Fig. 13. Upconversion emission spectra of the $GeO_2.9Nb_2O_5$:Ho^{3+}/Yb^{3+}/Tm^{3+} nanocomposite annealed at 900 °C for 3 h, under 980-nm excitation.

indicates that the nanocomposite structure is formed by several crystallites gathered.

Upconversion measurements were carried out under excitation at 980-nm of the $GeO_2.9Nb_2O_5$: Ho^{3+}/Yb^{3+}/Tm^{3+} calcined at 900 °C, depicted in Fig. 13. Emissions in the green (Ho^{3+} ions) and red (Ho^{3+} and Tm^{3+} ions) region are observed as previously described. The emission in the blue region is not observed when compared to Fig. 4B, which shows white light emission when excited at 980 nm. This indicates that only the $GeO_2.9Nb_2O_5$ structure does not have great influence on the spectroscopic properties for emission of white light and it is necessary to have this structure dispersed in the GeO_2 system, so that there is this contribution. Similarity can be seen in an analogous way in the GeO_2-Ta_2O_5:Er^{3+}/Yb^{3+} system, where the formation of $YbTaO_4$:Er^{3+} occurs, and this system alone does not have a high upconversion yield as its dispersed formation in the GeO_2-Ta_2O_5 host lattice [28].

Another point that is worth highlighting is the relationship of emissions in Fig. 13, red has a much more intense emission than green, and because it does not show emission in blue, which justifies that the distances between the Tm^{3+} and Ho^{3+} ions favor cross relaxation process. The same is depicted by Gouveia-Neto et al. [52] in SiO_2–Ta_2O_5: Ho^{3+}/Yb^{3+}/Tm^{3+} systems with increasing heat treatment temperature. Different from Fig. 4B that has issued RGB indicating that it is not occurring that energy transfer Tm^{3+} →Ho^{3+}, only energy transfer from Yb^{3+}→Tm^{3+} and Yb^{3+}→Ho^{3+}, possibly be in isolated environments in chemical environments $GeO_2.9Nb_2O_5$ and GeO_2, the cross-relaxation does not occur.

4. Conclusion

The $70GeO_2$-$30Nb_2O_5$ materials prepared by the sol–gel methodology, doped with 0.3Ho^{3+}/1.2 Yb^{3+}/0.5 Tm^{3+}, and thermally treated at different temperatures showed promising results. Trigonal GeO_2 was detected for all the samples, whereas a mixed oxide $GeO_2.9Nb_2O_5$ of tetragonal structure was obtained between 900 and 1100 °C, the stabilization of mixed oxide at high temperatures showed singular results as a rare earth host network with influence on luminescent properties. The luminescent properties were evaluated in samples calcined at 700, 900, and 1100 °C. Upconversion energy studies were carried out. The sample calcined at 900 °C emitted in the white light region and can be applied in cold white illumination. The sample treated at 1100 °C showed color purity greater than 96% in the yellow-green region and can be used in several photonic applications. However, it was verified that only $GeO_2.9Nb_2O_5$ has no influence on the generation of white light, the mixed oxide dispersed in GeO_2 is necessary to obtain this spectroscopic property.

Under excitation in the ultraviolet region (245–280 nm), the sample treated at 1100 °C stood out: it generated white light through modulation of the warm white illumination under excitation at longer ultraviolet wavelengths (275 and 280 nm) and cold white under excitation at shorter ultraviolet wavelengths (245–270 nm). In this sense, changes in the excitation wavelength can generate the quality of white light that is necessary for a given lighting environment. In this same material, the mixed oxide ($GeO_2.9Nb_2O_5$) influenced the emission band of the host lattice, which was different from the emission of the samples treated at other temperatures and indicated that formation of this mixed oxide influenced the spectroscopic properties of the material.

In conclusion, the sample treated at 900 °C and subjected to upconversion conditions and the sample treated at 1100 °C and under excitation in the ultraviolet have promising application in white light illumination.

Credit author statement

Vítor dos Santos de Souza: Methodology, Synthesis, Characterization, Spectroscopic measurements, made the figures, Data curation and Writing. **Fábio José Caixeta**: Spectroscopic measurements, Data curation and revised the manuscript. **Karmel de Oliveira Lima**: Spectroscopic measurements. **Rogéria Rocha Gonçalves**: Data curation, Supervision, Writing, review and editing.

Funding and acknowledgments

This work was supported by Conselho Nacional de Desenvolvimento Científico e Tecnológico (CNPq, 133,069/2020–6), Coordenação de

Aperfeiçoamento de Pessoal de Nível Superior (CAPES), and Fundação de Amparo à Pesquisa do Estado de São Paulo (FAPESP, Projects n° 2017/21,740–3, 2017/11,301–2, 2020/05319–9). RRG acknowledges CNPq for financial support (grant number: 303,110/2019–8). The authors would like to thank Cynthia Maria de Campos Prado Manso, who reviewed the text; and the Department of Chemistry – FFCLRP, University of São Paulo for the opportunity of using its facilities. We also thank Companhia Brasileira de Metalurgia e Mineração (CBMM) for supplying Nb_2O_5 and Photonics Nacional Instiurte for Science and Technology (INFO).

Declaration of competing interest

The authors declare that they have no known competing financial interests or personal relationships that could have appeared to influence the work reported in this paper.

References

[1] S. Bin Kwon, B.Y. Kim, I.S. Jang, S.W. Jeon, W.H. Kim, H.J. Jeong, J.P. Kim, M. K. Jung, B.W. Jeong, B.K. Kang, D.H. Yoon, Y.H. Song, Fabrication and luminous properties of phosphor ceramic for application in automotive laser headlight, Curr. Appl. Phys. 20 (2020) 862–865, https://doi.org/10.1016/j.cap.2020.04.001.

[2] H. Wang, Y. Mou, Y. Peng, Y. Zhang, A. Wang, L. Xu, H. Long, M. Chen, J. Dai, C. Chen, Fabrication of phosphor glass film on aluminum plate by using lead-free tellurite glass for laser-driven white lighting, J. Alloys Compd. 814 (2020) 152321, https://doi.org/10.1016/j.jallcom.2019.152321.

[3] H. Wu, Z. Hao, G.H. Pan, L. Zhang, H. Wu, X. Zhang, L. Zhang, J. Zhang, Phosphor-SiO_2 composite films suitable for white laser lighting with excellent color rendering, J. Eur. Ceram. Soc. 40 (2020) 2439–2444, https://doi.org/10.1016/j.jeurceramsoc.2020.01.020.

[4] C. Lee, M.S. Islim, S. Videv, A. Sparks, B. Shah, P. Rudy, M. McLaurin, H. Haas, J. Raring, Adv. LiFi Technol.: Laser light 1130213 (2020) 38, https://doi.org/10.1117/12.2537420.

[5] X. Zhou, P. Tian, C.W. Sher, J. Wu, H. Liu, R. Liu, H.C. Kuo, Growth, transfer printing and colour conversion techniques towards full-colour micro-LED display, Prog. Quant. Electron. 71 (2020) 100263, https://doi.org/10.1016/j.pquantelec.2020.100263.

[6] H. Zhang, Q. Su, S. Chen, Quantum-dot and organic hybrid tandem light-emitting diodes with multi-functionality of full-color-tunability and white-light-emission, Nat. Commun. 11 (2020) 1–8, https://doi.org/10.1038/s41467-020-16659-x.

[7] Y. Koinuma, R. Ishimatsu, H. Kuwae, K. Okada, J. Mizuno, T. Kasahara, White electrogenerated chemiluminescence using an anthracene derivative host and fluorescent dopants for microfluidic self-emissive displays, Sensors Actuators, A Phys. 306 (2020) 111966, https://doi.org/10.1016/j.sna.2020.111966.

[8] Y. Zhu, J. Zhu, H. Song, J. Huang, Z. Lu, G. Pan, Samarium doping improves luminescence efficiency of $Cs_3Bi_2Br_9$ perovskite quantum dots enabling efficient white light-emitting diodes, J. Rare Earths (2020) 3–8, https://doi.org/10.1016/j.jre.2020.06.007.

[9] M. Wang, Y. Zhang, Z. Hu, J. Zhang, A single-phased $Ca_4(PO_4)_2O$: Tm^{3+}, Tb^{3+}, Eu^{2+} white light-emitting phosphor with tunable emission color, J. Lumin. 224 (2020) 117301, https://doi.org/10.1016/j.jlumin.2020.117301.

[10] Z. Meng, S. Zhang, S. Wu, Power density dependent upconversion properties of $NaYbF_4$: Er^{3+}@$NaYbF_4$: Tm^{3+}@$NaYF_4$ nanoparticles and their application in white-light emission LED, J. Lumin. 227 (2020) 117566, https://doi.org/10.1016/j.jlumin.2020.117566.

[11] G. Lozano, O.B. Silva, W. Faria, A.S.S. de Camargo, R.R. Gonçalves, D. Manzani, R. Bruna, V.A.G. Rivera, E. Marega, Cold white light emission in tellurite-zinc glasses doped with Er^{3+}–Yb^{3+}–Tm^{3+} under 980 nm, J. Lumin. 228 (2020) 117538, https://doi.org/10.1016/j.jlumin.2020.117538.

[12] O. Soriano-Romero, R. Lozada-Morales, A.N. Meza-Rocha, S. Carmona-Téllez, U. Caldiño, B. Flores-Desirena, R. Palomino-Merino, Cold bluish white and blue emissions in Cu^{+}-doped zinc phosphate glasses, J. Lumin. 217 (2020) 1–7, https://doi.org/10.1016/j.jlumin.2019.116791.

[13] S.K. Gupta, J.P. Zuniga, M. Abdou, M.P. Thomas, M. De Alwis Goonatilleke, B. S. Guiton, Y. Mao, Lanthanide-doped lanthanum hafnate nanoparticles as multicolor phosphors for warm white lighting and scintillators, Chem. Eng. J. 379 (2020) 122314, https://doi.org/10.1016/j.cej.2019.122314.

[14] N. Deopa, M.K. Sahu, P.R. Rani, R. Punia, A.S. Rao, Realization of warm white light and energy transfer studies of Dy^{3+}/Eu^{3+} co-doped Li_2O-PbO-Al_2O_3-B_2O_3 glasses for lighting applications, J. Lumin. 222 (2020) 117166, https://doi.org/10.1016/j.jlumin.2020.117166.

[15] X. Bai, G. Caputo, Z. Hao, V.T. Freitas, J. Zhang, R.L. Longo, O.L. Malta, R.A. S. Ferreira, N. Pinna, Efficient and tuneable photoluminescent boehmite hybrid nanoplates lacking metal activator centres for single-phase white LEDs, Nat. Commun. 5 (2014) 1–8, https://doi.org/10.1038/ncomms6702.

[16] W. Bao, X.Y. Yu, W.W. Dong, J. Zhao, Z.F. Tian, D.S. Li, Novel composites of graphitic-phase nitrogen carbon/lanthanide coordination polymers as white light-emitting phosphor, Zeitschrift Fur Anorg. Und Allg. Chemie. 645 (2019) 1279–1284, https://doi.org/10.1002/zaac.201900245.

[17] V. Roud, A. Sokolov, D. Meissner, Nanotechnology for high-tech industries: light-emitting diodes, in: first ed., in: D. Meissner, L. Gokhberg, O. Saritas (Eds.), Emerg. Technol. Econ. Dev., Springer International Publishing, 2019, pp. 49–75, https://doi.org/10.1007/978-3-030-04370-4.

[18] Z. Xie, X. Liu, W. Zhao, Tunable photoluminescence and energy transfer of novel phosphor $Sr_9La_2W_4O_{24}$:Sm^{3+}, Eu^{3+} for near-UV white LEDs, J. Mater. Sci. Mater. Electron. 31 (2020) 7114–7122, https://doi.org/10.1007/s10854-020-03282-1.

[19] X. Chen, Y. An, X. Chang, W. Xiao, A new cadmium rare-earth oxyborate $Cd_4DyO(BO_3)_3$ and luminescent properties of the Cd_4Dy1-$xSmxO(BO_3)_3$ ($0 \leq x \leq 0.8$) phosphors, J. Solid State Chem. 295 (2021) 121944, https://doi.org/10.1016/j.jssc.2020.121944.

[20] C.C. Lin, A. Meijerink, R.S. Liu, Critical red components for next-generation white LEDs, J. Phys. Chem. Lett. 7 (2016) 495–503, https://doi.org/10.1021/acs.jpclett.5b02433.

[21] Y. Yang, B. Liu, Y. Zhang, X. Lv, L. Wei, J. Xu, H. Zhang, X. Wang, C. Zhang, J. Li, Influence of Mg^{2+}/Ga^{3+} doping on luminescence of $Y_3Al_5O_{12}$:Ce^{3+} phosphors, J. Mater. Sci. Mater. Electron. 29 (2018) 17154–17159, https://doi.org/10.1007/s10854-018-9806-5.

[22] J. Ma, L.M. Zhao, C.Y. Jin, B. Yan, Luminescence responsive composites of rare earth metal-organic frameworks covalently linking microsphere resin, Dyes Pigments 173 (2020) 107883, https://doi.org/10.1016/j.dyepig.2019.107883.

[23] P. Du, W. Ran, C. Wang, L. Luo, W. Li, Facile realization of boosted near-infrared-visible light driven photocatalytic activities of BiOF nanoparticles through simultaneously exploiting doping and upconversion strategy, Adv. Mater. Interfac. 8 (2021) 1–12, https://doi.org/10.1002/admi.202100749.

[24] P. Du, L. Luo, W. Li, F. Yan, G. Xing, Multi-site occupancies and photoluminescence characteristics in developed Eu^{2+}-activated $Ba_5SiO_4Cl_6$ bifunctional platform: towards manufacturable optical thermometer and indoor illumination, J. Alloys Compd. 826 (2020) 154233, https://doi.org/10.1016/j.jallcom.2020.154233.

[25] P. Du, mai J. Tang, W. Li, L. Luo, Exploiting the diverse photoluminescence behaviors of $NaLuF_4$:xEu^{3+} nanoparticles and g-C_3N_4 to realize versatile applications in white light-emitting diode and optical thermometer, Chem. Eng. J. 406 (2021) 127165, https://doi.org/10.1016/j.cej.2020.127165.

[26] S.K. Gupta, J.P. Zuniga, M. Abdou, M.P. Thomas, M. De Alwis Goonatilleke, B. S. Guiton, Y. Mao, Lanthanide-doped lanthanum hafnate nanoparticles as multicolor phosphors for warm white lighting and scintillators, Chem. Eng. J. 379 (2020) 122314, https://doi.org/10.1016/j.cej.2019.122314.

[27] A. Jha, B. Richards, G. Jose, T. Teddy-Fernandez, P. Joshi, X. Jiang, J. Lousteau, Rare-earth ion doped TeO_2 and GeO_2 glasses as laser materials, Prog. Mater. Sci. 57 (2012) 1426–1491, https://doi.org/10.1016/j.pmatsci.2012.04.003.

[28] F.J. Caixeta, A.R.N. Bastos, A.M.P. Botas, L.S. Rosa, V.S. Souza, A.N. Carneiro Neto, A. Ferrier, P. Goldner, L.D. Carlos, R.R. Gonçalves, R.A.S. Ferreira, High-quantum yield upconverting Er^{3+}/Yb^{3+} organic-inorganic hybrid dual coatings for real-time temperature sensing and photothermal conversion, J. Phys. Chem. C 124 (2020) 19892–19903, https://doi.org/10.1021/acs.jpcc.0c03874.

[29] R.R. Pereira, F.T. Aquino, A. Ferrier, P. Goldner, R.R. Gonçalves, Nanostructured rare earth doped Nb_2O_5: structural, optical properties and their correlation with photonic applications, J. Lumin. 170 (2016) 707–717, https://doi.org/10.1016/j.jlumin.2015.08.068.

[30] T. Blanquart, J. Niinistö, M. Heikkilä, T. Sajavaara, K. Kukli, E. Puukilainen, C. Xu, W. Hunks, M. Ritala, M. Leskelä, Evaluation and comparison of novel precursors for atomic layer deposition of Nb_2O_5 thin films, Chem. Mater. 24 (2012) 975–980, https://doi.org/10.1021/cm2026812.

[31] F.F. Sene, J.R. Martinelli, L. Gomes, Optical and structural characterization of rare earth doped niobium phosphate glasses, J. Non-Cryst. Solids 348 (2004) 63–71, https://doi.org/10.1016/j.jnoncrysol.2004.08.127.

[32] L. Petit, T. Cardinal, J.J. Videau, E. Durand, L. Canioni, M. Martines, Y. Guyot, G. Boulon, Effect of niobium oxide introduction on erbium luminescence in borophosphate glasses, Opt. Mater. 28 (2006) 172–180, https://doi.org/10.1016/j.optmat.2004.12.007.

[33] F.J. Caixeta, F.T. Aquino, R.R. Pereira, R.R. Gonçalves, Broad and intense NIR luminescence from rare earth doped SiO_2-Nb_2O_5 glass and glass ceramic prepared by a new sol gel route, J. Lumin. 171 (2016) 63–71, https://doi.org/10.1016/j.jlumin.2015.08.054.

[34] J. Haines, J. Léger, C. Chateau, Transition to a crystalline high-pressure phase in at room temperature, Phys. Rev. B Condens. Matter 61 (2000) 8701–8706, https://doi.org/10.1103/PhysRevB.61.8701.

[35] J. Haines, O. Cambon, E. Philippot, L. Chapon, S. Hull, A neutron diffraction study of the thermal stability of the α-quartz-type structure in germanium dioxide, J. Solid State Chem. 166 (2002) 434–441, https://doi.org/10.1006/jssc.2002.9625.

[36] B. Park, The structure of germanium niobium oxide, an inherently non-stoichiometric 'block' structure, Proc. R. Soc. London. A. Math. Phys. Sci. 346 (1975) 139–156, https://doi.org/10.1098/rspa.1975.0170.

[37] F.T. Aquino, R.R. Pereira, J.L. Ferrari, S.J.L. Ribeiro, A. Ferrier, P. Goldner, R. R. Gonçalves, Unusual broadening of the NIR luminescence of Er^{3+}-doped Nb_2O_5 nanocrystals embedded in silica host: preparation and their structural and spectroscopic study for photonics applications, Mater. Chem. Phys. 147 (2014) 751–760, https://doi.org/10.1016/j.matchemphys.2014.06.016.

[38] D.V. Balitsky, V.S. Balitsky, D.Y. Pushcharovsky, G.V. Bondarenko, A.V. Kosenko, Growth and characterization of GeO_2 single crystals with the quartz structure, J. Cryst. Growth 180 (1997) 212–219, https://doi.org/10.1016/S0022-0248(97)00224-8.

[39] A. Pawlicka, M. Atik, M.A. Aegerter, Synthesis of multicolor Nb_2O_5 coatings for electrochromic devices, Thin Solid Films 301 (1997) 236–241, https://doi.org/10.1016/S0040-6090(96)09583-1.

[40] D.C. Calabro, E.W. Valyocsik, F.X. Ryan, In situ ATR/FTIR study of mesoporous silicate syntheses, Microporous Mater. 7 (1996) 243–259, https://doi.org/10.1016/S0927-6513(96)00045-4.
[41] D.R. Scheuing, J.G. Weers, Characterization of viscoelastic surfactant mixtures part I: Fourier transform infrared spectroscopic studies, Colloid. Surface. 55 (1991) 41–56, https://doi.org/10.1016/0166-6622(91)80081-X.
[42] P. Pascuta, E. Culea, FTIR spectroscopic study of some bismuth germanate glasses containing gadolinium ions, Mater. Lett. 62 (2008) 4127–4129, https://doi.org/10.1016/j.matlet.2008.06.015.
[43] L.Y. Zhang, H. Li, L.L. Hu, Statistical structure analysis of GeO_2 modified Yb^{3+}: phosphate glasses based on Raman and FTIR study, J. Alloys Compd. 698 (2017) 103–113, https://doi.org/10.1016/j.jallcom.2016.12.175.
[44] F.J. Caixeta, F.T. Aquino, R.R. Pereira, R.R. Gonçalves, Niobium oxide influence on the structural properties and NIR luminescence of Er3+/Yb3+ co-doped and single-doped $1-xSiO_2-xNb_2O_5$ nanocomposites prepared by an alternative sol–gel route, J. Lumin. 180 (2016) 355–363, https://doi.org/10.1016/j.jlumin.2016.08.057.
[45] H. Wang, J. Li, J. Sun, Y. Wang, Z. Liang, P. Ma, D. Zhang, J. Wang, J. Niu, Synthesis, structure, and luminescent properties of a family of lanthanide-functionalized peroxoniobiophosphates, Sci. Rep. 7 (2017) 2–10, https://doi.org/10.1038/s41598-017-10811-2.
[46] A. Pandey, V.K. Rai, Colour emission tunability in Ho^{3+}-Tm^{3+}-Yb^{3+} co-doped Y2O3 upconverted phosphor, Appl. Phys. B Laser Opt. 109 (2012) 611–616, https://doi.org/10.1007/s00340-012-5224-1.
[47] L. Xing, W. Yang, J. Lin, M. Huang, Y. Xue, Enhanced and stable upconverted white-light emission in Ho^{3+}/Yb^{3+}/Tm^{3+}-doped $LiNbO_3$ single crystal via Mg^{2+} ion doping, Sci. Rep. 7 (2017) 1–7, https://doi.org/10.1038/s41598-017-15367-9.
[48] Q. Wang, G. Zhu, Y. Li, Y. Wang, Photoluminescent properties of Pr^{3+} activated Y_2WO_6 for light emitting diodes, Opt. Mater. 42 (2015) 385–389, https://doi.org/10.1016/j.optmat.2015.01.032.
[49] Y. Shi, Y. Wen, M. Que, G. Zhu, Y. Wang, Structure, photoluminescent and cathodoluminescent properties of a rare-earth free red emitting β-$Zn_3B_2O_6$:Mn^{2+} phosphor, Dalton Trans. 43 (2014) 2418–2423, https://doi.org/10.1039/c3dt52405a.
[50] F. Caixeta, Fábio Thomaz, R. Ramiro, Highly red luminescent Nb_2O_5 : Eu^{3+} nanoparticles in silicate host for solid-state lighting and energy conversion, Opt. Mater. 111 (2020) 3–9, https://doi.org/10.1016/j.optmat.2020.110671.
[51] W.C. Muscelli, K.D.O. Lima, F. Thomaz Aquino, R.R. Gonçalves, Blue and NIR emission from nanostructured Tm^{3+}/Yb^{3+} co-doped SiO_2-Ta_2O_5 for photonic applications, J. Phys. D Appl. Phys. 49 (2016) 175107, https://doi.org/10.1088/0022-3727/49/17/175107.
[52] A.S. Gouveia-Neto, L.A. Bueno, E.B. Da Costa, E.A. Silva, J.L. Ferrari, K.O. Lima, R. R. Gonçalves, Generation of wide color gamut visible light in rare-earth triply doped tantalum oxide crystalline ceramic powders, J. Appl. Phys. 107 (2010) 10–13, https://doi.org/10.1063/1.3430998.
[53] E. Osiac, I. Sokólska, S. Kück, Upconversion-induced blue, green and red emission in Ho^{3+}:BaY_2F_8, J. Alloys Compd. 323–324 (2001) 283–287, https://doi.org/10.1016/S0925-8388(01)01110-0.
[54] H.U.G.M. Pollnau, D.R. Gamelin, S.R. Luthi, Power dependence of upconversion luminescence in lanthanide and transition-metal-ion systems, Phys. Rev. B 61 (2000) 3337, https://doi.org/10.1103/PhysRevB.61.3337.
[55] G. Li, C. Li, Z. Xu, Z. Cheng, J. Lin, Facile synthesis, growth mechanism and luminescence properties of uniform $La(OH)_3$:Ho^{3+}/Yb^{3+} and La_2O_3:Ho^{3+}/Yb^{3+} nanorods, CrystEngComm 12 (2010) 4208–4216, https://doi.org/10.1039/c0ce00075b.
[56] Y. Su, G. Li, X. Chen, J. Liu, P. Li, Hydrothermal synthesis of $GdVO_4$:Ho^{3+} Nanorods with a novel white-light emission, Chem. Lett. 37 (2008) 762–763, https://doi.org/10.1246/cl.2008.762.
[57] M. Zhang, H. Wen, X. Pan, J. Yu, H. Shao, F. Ai, H. Yu, M. Tang, L. Gai, Study on upconversion and thermal properties of Tm^{3+}/Yb^{3+} co-doped La_2O_3-Nb_2O_5-Ta_2O_5 glasses, Materials 11 (2018) 1–8, https://doi.org/10.3390/ma11081352.
[58] J. Wang, Y. Bu, X. Wang, H.J. Seo, Optical thermometry in low temperature through manipulating the energy transfer from WO_6^{6-} to Ho^{3+} in Y_2WO_6:Ho^{3+} phosphors, Opt. Mater. 84 (2018) 778–785, https://doi.org/10.1016/j.optmat.2018.08.009.
[59] A. Pandey, V.K. Rai, R. Dey, K. Kumar, Enriched green upconversion emission in combustion synthesized Y_2O_3:Ho^{3+}-Yb^{3+} phosphor, Mater. Chem. Phys. 139 (2013) 483–488, https://doi.org/10.1016/j.matchemphys.2013.01.043.
[60] V.C. Adya, M. Mohapatra, M.K. Bhide, V. Natarajan, Observation of "cool daylight" white light emission from Eu and Tb co-doped $SrMoO_4$ nano ceramics, Mater. Sci. Eng. B Solid-State Mater. Adv. Technol. 203 (2016) 35–40, https://doi.org/10.1016/j.mseb.2015.10.010.
[61] R.V. Perrella, M.G. Manfré, R.R. Gonçalves, G.H. Silva, J.H. Faleiro, H.P. Barbosa, C.A. de Oliveira, M.A. Schiavon, J.L. Ferrari, Dipole-dipole energy transfer mechanism to the blue-white-red color-tunable emission presented by $CaYAlO_4$: Tb^{3+},Eu^{3+} biocompatibility material obtained by the simple and low cost of chemical route, Mater. Chem. Phys. 247 (2020) 122855, https://doi.org/10.1016/j.matchemphys.2020.122855.
[62] C.S. McCamy, Correlated color temperature as an explicit function of chromaticity coordinates, Color Res. Appl. 17 (1992) 142–144, https://doi.org/10.1002/col.5080170211.
[63] A.L. Patterson, The scherrer formula for X-ray particle size determination, Phys. Rev. 56 (1939) 978–982, https://doi.org/10.1103/PhysRev.56.978.
[64] F.F. Ferreira, E. Granado, W. Carvalho, S.W. Kycia, D. Bruno, R. Droppa, X-ray powder diffraction beamline at D10B of LNLS: application to the Ba_2FeReO_6 double perovskite, J. Synchrotron Radiat. 13 (2006) 46–53, https://doi.org/10.1107/S0909049505039208.
[65] F.T. Aquino, F.J. Caixeta, K. de Oliveira Lima, M. Kochanowicz, D. Dorosz, R. R. Gonçalves, Broadband NIR emission from rare earth doped-SiO_2-Nb_2O_5 and SiO2-Ta_2O_5 nanocomposites, J. Lumin. 199 (2018) 138–142, https://doi.org/10.1016/j.jlumin.2018.03.018.
[66] J.L. Ferrari, K.O. Lima, L.J.Q. Maia, S.J.L. Ribeiro, R.R. Gonaçalves, Structural and spectroscopic properties of luminescent Er^{3+}-doped SiO_2-Ta_2O_5 nanocomposites, J. Am. Ceram. Soc. 94 (2011) 1230–1237, https://doi.org/10.1111/j.1551-2916.2010.04191.x.
[67] N.D. Afify, G. Dalba, F. Rocca, XRD and EXAFS studies on the structure of Er3+-doped SiO_2-HfO_2 glass-ceramic waveguides: Er^{3+}-activated HfO_2 nanocrystals, J. Phys. D Appl. Phys. 42 (2009) 115416, https://doi.org/10.1088/0022-3727/42/11/115416.
[68] L.M. Marcondes, S. Maestri, B. Sousa, R.R. Gonçalves, F.C. Cassanjes, G.Y. Poirier, High niobium oxide content in germanate glasses: thermal, structural, and optical properties, J. Am. Ceram. Soc. 101 (2018) 220–230, https://doi.org/10.1111/jace.15215.
[69] F.M.F. Filho, R.R. Gonçalves, S.J.L. Ribeiro, L.J.Q. Maia, Structural and optical properties of Er^{3+} doped SiO_2-Al_2O_3-GeO_2 compounds prepared by a simple route, Mater. Sci. Eng. B Solid-State Mater. Adv. Technol. 194 (2015) 21–26, https://doi.org/10.1016/j.mseb.2014.12.023.